Contactless Determination of the Photoconductivity Action Spectrum, Exciton Diffusion Length, and Charge Separation Efficiency in Polythiophene-Sensitized TiO_2 Bilayers

Jessica E. Kroeze, Tom J. Savenije,* Martien J. W. Vermeulen, and John M. Warman

Radiation Chemistry Department, IRI, Delft University of Technology, Mekelweg 15, 2629 JB Delft, The Netherlands

Received: July 31, 2002; In Final Form: April 16, 2003

The flash-photolysis time-resolved microwave conductivity technique (FP-TRMC) has been used to study photoinduced charge separation in bilayers consisting of a smooth, transparent, 80 nm thick layer of anatase TiO_2 onto which poly(3-hexylthiophene) (P3HT) sensitizer layers have been spin-coated. Interfacial charge separation, resulting from excitation of the polymer in the visible, is found to persist well into the millisecond time domain. Photoconductivity action spectra have been measured between 420 and 700 nm for P3HT layer thicknesses, L, from ~2 to 200 nm. Using this electrodeless technique, the bilayers could be irradiated from either the polymer ("front") or semiconductor ("back") side. On front-side irradiation at 540 nm (close to the absorption maximum of the polymer), the efficiency of charge separation per incident photon (IPCSE) initially increased to a maximum value of 0.8% for $L \approx 10$ nm. For thicker layers the IPCSE gradually decreased, eventually to 0.1% for $L \approx 170$ nm. On back-side irradiation the IPCSE increased over the first 10 nm to a value close to the maximum found for front-side irradiation, and decreased only slightly for further increase in layer thickness. Analytical expressions for the thickness dependence based on exciton diffusion with a Lambert−Beer excitation profile have been used to fit the experimental data. Best fits were obtained for an exciton diffusion length, Λ ($=\sqrt{(D\tau)}$ with D the diffusion coefficient and τ the natural lifetime), of 5.3 or 2.6 nm depending on whether excitons were taken to be reflected or quenched at the polymer/gas interface, respectively. The IPCSE decreased at high light intensities; an effect that is attributed to the occurrence of exciton−exciton annihilation within the polymer layer.

Introduction

Their strong optical absorptions in the visible make conjugated polymers, such as derivatives of phenylene−vinylene (PPVs) and thiophene (PTs), potential candidates for application as antenna layers for the photovoltaic conversion of solar energy. Initial studies focused on the use of PPVs to form photovoltaic cells based on the formation of a Schottky barrier or p/n heterojunction.[1−6] The efficiencies were fairly low, however, and an improvement in performance was achieved by the formation of so-called bulk heterojunctions, consisting of a blend of the conducting polymer with molecules such as fullerenes,[7,8] perylenediimides,[9] or electron-accepting conjugated polymers.[10] Recently, heterojunctions based on a bilayer of a conjugated polymer and a wide-band-gap semiconductor have also been described.[11−17]

At present, the use of thiophenes in different kinds of photoactive layers is being intensively studied. Bulk heterojunctions of thiophenes and fullerenes have been found to be promising candidates for application in solar energy devices.[7,18−24] In addition, junctions based on organized layers of thiophenes forming a heterojunction with organic[25−27] and inorganic[28−32] films have been investigated. Polythiophenes have certain advantages over PPVs, since thin films of substituted PTs are claimed to have self-organizing properties depending on the backbone substituents and the regioregularity.[33−35] Furthermore, the optical properties of PTs can be readily tailored via substitution on the main chain to obtain low-band-gap materials.[36,37] Another important property of PTs that makes them particularly suitable for solar cell applications is their enhanced photostability compared with that of PPVs.

Photovoltaic studies on junctions consisting of PTs or PPVs deposited on a wide-band-gap semiconductor such as TiO_2 have shown that on excitation of the polymer layer electrons are injected into the conduction band of the TiO_2, as depicted in Figure 1B.[11−14,28,30] In this way the polymer acts as a sensitizer to visible light for the semiconductor. The mechanism of charge separation in such a photovoltaic cell is based on the creation of neutral photoexcitations in the bulk of the polymer film which reach the interface by exciton diffusion: processes 1 and 3 in Figure 1B. At the interface, electron injection into the conduction band of the semiconductor occurs and the resulting charge carriers can diffuse away from the interface and be collected at the electrodes (not shown in Figure 1).

In such a device the polymer has a dual function, as both sensitizer and hole transport layer. The fact that no liquid phase is required should be advantageous for the long-term stability compared with the original Grätzel type solar cell.[38,39] This approach, however, makes several demands on the properties of the organic antenna layer; it must have (a) a strong and broad absorption within the solar energy spectrum, (b) a large exciton diffusion length, (c) a high efficiency for electron injection at the interface, and (d) a high mobility for positive charge carriers.

The exciton diffusion length, $\Lambda = \sqrt{(D\tau)}$, with D the exciton diffusion coefficient and τ the natural exciton lifetime, is a parameter of prime importance in simple bilayer structures because photoexcitations created initially in the bulk of the antenna layer must be able to diffuse within their lifetime to

10.1021/jp0217738 CCC: $25.00
Published on Web 07/04/2003

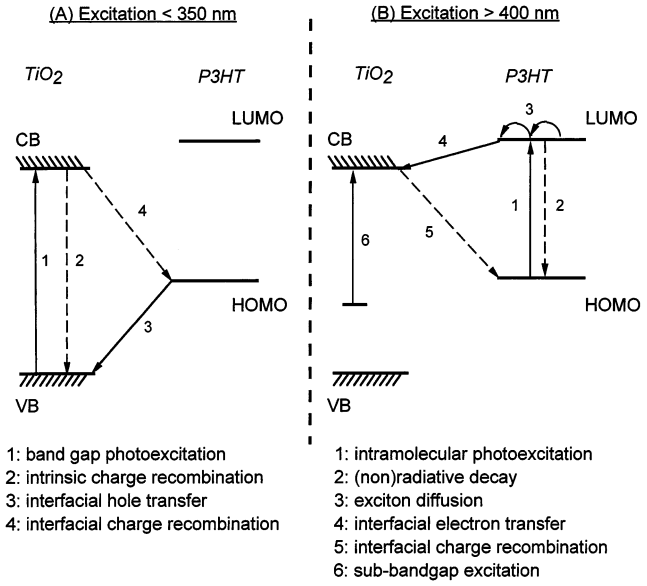

Figure 1. Schematic representations of the photophysical processes underlying interfacial charge separation in a TiO_2/P3HT bilayer for light of wavelengths shorter than 350 nm (left) and longer than 400 nm (right).

the semiconductor interface over a distance which is comparable with the photon penetration depth, $\Lambda_{hv} = 1/\alpha$, with α the exponential linear absorption coefficient. The values of Λ_{hv}, even at the maximum of the visible absorption bands of conjugated polymers, are usually on the order of 100 nm. Exciton diffusion lengths of tens to hundreds of nanometers are therefore required in order to ensure a reasonably high efficiency of charge separation. While values of Λ as large as microns have been reported for (poly)crystalline organic materials from fluorescence quenching measurements,[40−42] much lower values have been estimated for conjugated polymeric materials. For example, for PPV derivatives Λ has been estimated to be $\sim$20 nm.[11,43,44] For polythiophenes values of $\sim$5 nm have been reported on the basis of an analysis of the photovoltaic characteristics of a heterojunction cell[27] and the fluorescence quenching in a polythiophene/fullerene bilayer.[45]

Attempts to circumvent the exciton diffusion length problem associated with bilayer structures have led to the use of nanoporous semiconductor layers and blends. Even in these systems, however, the value of Λ still plays a role, since it determines the maximum amount of the antenna material that can be incorporated while retaining a high charge separation efficiency.

The determination of Λ from photovoltaic measurements is complicated by factors such as exciton deactivation at the cathode, nonohmic electrode contacts, optical filter effects, and pinhole defects in the photoactive layers. To avoid these problems, we have devised a method of determining Λ which does not require the application of electrode layers and hence is free from most of these complications. In this method, a layer of the organic antenna compound is spin-coated onto a smooth, polycrystalline layer of anatase TiO_2. The photoconductivity of the bilayer resulting on flash-photolysis is then monitored using the time-resolved microwave conductivity technique (TRMC). Since the mobility of electrons in the TiO_2 layer is orders of magnitude larger than that of charge carriers in the organic layer, substantial photoconductivity transients are only observed when electron injection into the conduction band of the semiconductor occurs. Because of the well-defined interfacial region, a measure of Λ can be obtained by monitoring the photoconductivity as a function of the thickness of the antenna layer. Information can also be obtained on the wavelength dependence of the photoconductivity (the action spectrum), the efficiency of interfacial charge separation, and the time scale of charge recombination. The application of the method is illustrated in the present paper with results obtained using regioregular poly(3-hexylthiophene) as the antenna layer.

Experimental Section

Sample Preparation. 92% regioregular poly(3-hexylthiophene) (P3HT) was synthesized in the group of prof R. A. J. Janssen, Eindhoven University, and was used as received. Thin films ($\sim$80 nm thick) of anatase TiO_2 were deposited on 1 mm thick, 12 × 25 mm^2 quartz plates (ESCO products) by electron beam evaporation, yielding smooth, transparent layers as described previously.[46] After a 24 h annealing period in air at 450 °C, a homogeneous, optically clear film of P3HT was deposited at room temperature by spin-coating a solution in $CHCl_3$ at a spin velocity of 1800 rpm. The film thickness, L, was varied from 2 to 200 nm by using solutions varying in concentration from 0.1 to 10 mg/mL.

Optical Characterization. A Perkin-Elmer "Lambda 900" UV/vis/NIR spectrophotometer equipped with an integrating sphere ("Labsphere") was used to measure the fraction of incident light reflected and transmitted by the sample, F_R and F_T, respectively. The optical density of the sample is given by

$$\mathrm{OD} = -\log_{10}\left(\frac{F_T}{1 - F_R}\right) \tag{1}$$

The absorption spectra, OD(λ), for TiO_2 and P3HT layers alone and a TiO_2/P3HT bilayer are shown in Figure 2, for light incident on the gas or quartz substrate side of the sample ("front-" or "back-side" illumination). Absorption spectra are shown in Figure 3 for P3HT layers with different layer thicknesses prepared using the same conditions of spin-coating as in the preparation of the bilayers.

A parameter that is more relevant than the optical density for comparison with the wavelength-dependent photoconductivity transients is the fraction F_A of incident photons which is actually absorbed within the sample. This can be derived from the spectrophotometric measurements via

$$F_A = 1 - (F_R + F_T) \tag{2}$$

$F_A(\lambda)$ is denoted here as the "attenuation spectrum" to differentiate it from the "absorption spectrum", OD(λ).

The absorption of light by thin layers of solid materials is most conveniently treated mathematically in terms of the exponential linear absorption coefficient, α, which, for a layer thickness L, is defined by

$$\frac{F_T}{(1 - F_R)} = \mathrm{e}^{-\alpha L} \tag{3}$$

From eqs 1 and 3, α is seen to be related to the optical density by

$$\alpha = \frac{\mathrm{OD}}{L} \ln 10 \tag{4}$$

Using a step-profiler (Dektak 3ST) to measure the film thickness for some of the samples, a value of $\alpha = 1.6 \times 10^7\ m^{-1}$ at 540 nm was determined for P3HT from the spectrophotometric data. This value was used to estimate the layer thickness for the other samples from their measured optical densities at 540 nm. This

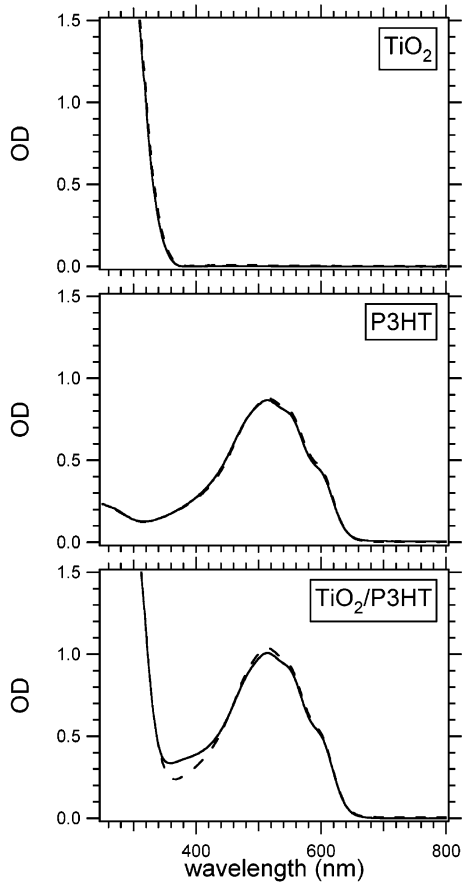

Figure 2. Optical absorption spectra of single layers of TiO_2 (ca. 80 nm) and P3HT (ca. 100 nm), and a TiO_2/P3HT bilayer. Full and dashed lines: illumination from the gas ("front") or quartz substrate ("back") sides of the sample, respectively.

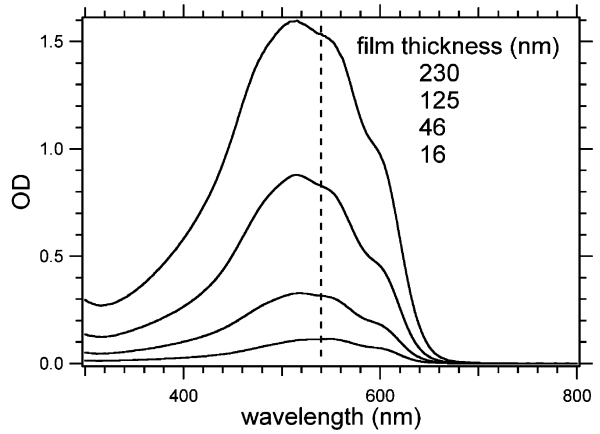

Figure 3. Optical absorption spectra of spin-coated layers of P3HT of different thickness. The vertical dashed line corresponds to 540 nm, the excitation wavelength used for the thickness-dependence measurements.

value of α corresponds to a photon penetration depth, that is, the depth at which the intensity is reduced to 1/e of its initial value, of $\Lambda_{hv} = 63$ nm.

Flash-Photolysis Time-Resolved Microwave Conductivity (FP-TRMC). Immediately after preparation, the samples were mounted in an X-band microwave cavity at a position corresponding to a maximum in the electric field strength of the standing wave pattern at resonance, as shown in Figure 4. The sample could be illuminated via a grating in the copper endplate of the cavity which was covered and vacuum sealed with a quartz window. The samples could be reversed, allowing illumination of bilayers from either the P3HT ("front") or TiO_2 ("back") side. The iris coupling hole of the cavity was sealed with a polyimide foil. The cavity was attached to a vacuum line, and the air was replaced by a mixture of 10% SF_6 in CO_2 at atmospheric pressure to scavenge any free electrons which might be ejected from the film by photoelectron emission.[47]

For photoexcitation in the visible, the third harmonic of a Q-switched Nd:YAG laser ("Infinity 15-30", Coherent) was used to pump an optical parametric oscillator (OPO), yielding 3 ns fwhm pulses continuously tunable from 420 to 700 nm. For wavelengths in the UV, the visible light pulses from the OPO were frequency doubled by a second harmonic generator (SHG). The remaining visible light was deflected from the beam using a Glan-Taylor polarizer. The beam was expanded using CaF_2 lenses to give a close to uniform intensity over a rectangular area of $\sim 1 \times 2$ cm^2, close to the cross-sectional dimensions of the cavity and the sample. The total number of incident photons per unit area per pulse, I_0, was derived from the pulse power, which was monitored by reflecting a small, known percentage of the light onto the pyroelectric sensor of a Labmaster power meter (Coherent). The intensity of the laser beam could be attenuated using a series of metal-coated neutral-density filters (Melles Griot) in tandem, yielding I_0 values in the range 1×10^{12} to 2×10^{14} photons/cm^2 per pulse.

Any photoinduced change in the conductivity of the sample was monitored as a change in the microwave power reflected by the cavity using nanosecond time-response microwave circuitry and detection equipment described previously.[48] TRMC transients were stored using either a Tektronix TDS 680 or a Sony/Tektronix RTD 710A transient digitizer. The former was used to record data over the first few hundred nanoseconds with a linear time-base and digital time resolution better than 1 ns. The latter was used to store data with a logarithmic time-base which allowed transients to be monitored from 10 ns to 10 ms using a single laser pulse, with, however, diminished time-resolution at early times. The overall time response was determined mainly by the 18 ns response time of the microwave resonant cavity used.

In the following section the application of the FP-TRMC technique to thin-film samples is discussed in more detail.

Data Analysis. The change in microwave power reflected by the microwave cavity as a result of a change in conductivity of the irradiated film, $\Delta\sigma$, is given by

$$\frac{\Delta P}{P} = -K\int_0^L \Delta\sigma(z)\,\partial z \tag{5}$$

where K is the known sensitivity factor of the cavity. The conductivity change at depth z within the film is related to the concentration of charge carrier pairs formed, N_p, and the sum of the mobilities, $\Sigma\mu$, by

$$\Delta\sigma(z) = eN_p(z)\sum\mu \tag{6}$$

If $\delta F_A(z)$ is the fraction of incident photons absorbed within a thin layer between z and $z + \delta z$ (see Figure 5), and I_0 is the integrated number of incident photons per unit area in the pulse, then the end of pulse concentration, in the absence of decay within the pulse, is given by

$$N_p(z) = \frac{I_0\phi_{CS}(z)\,\partial F_A(z)}{\partial z} \tag{7}$$

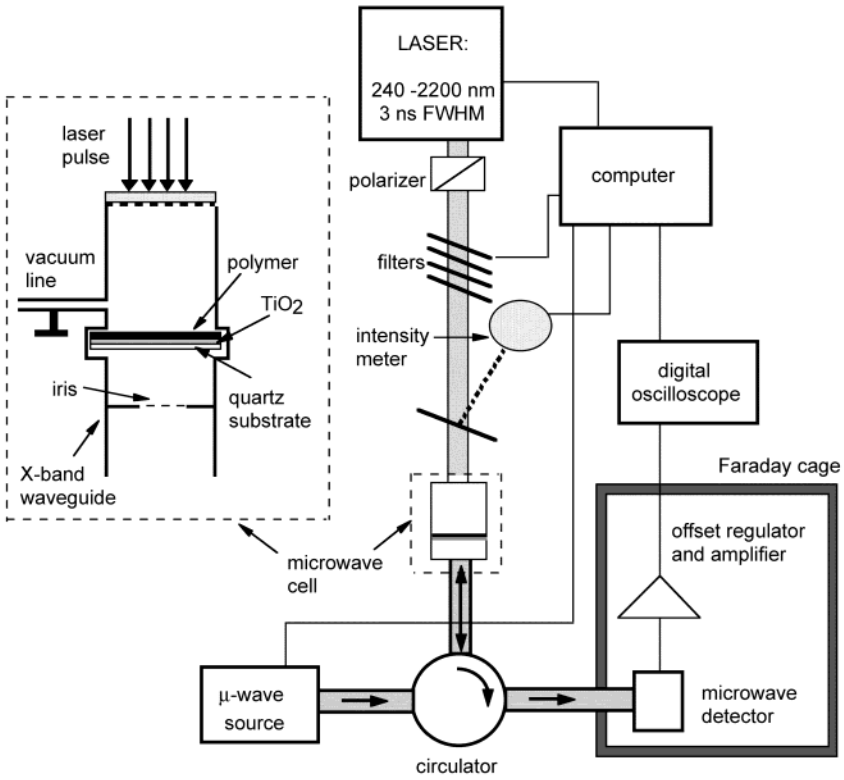

Figure 4. Schematic representation of the flash-photolysis time-resolved microwave conductivity apparatus and the sample conditions in the microwave cavity for front-side irradiation.

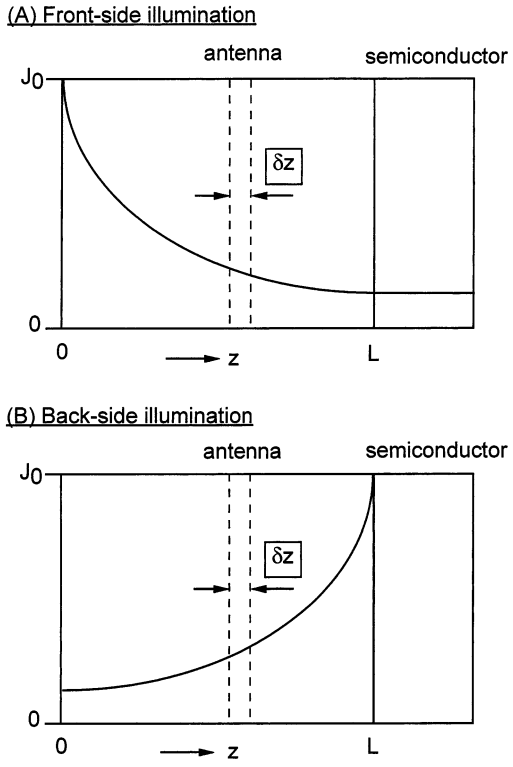

Figure 5. Excitation profiles within an antenna layer of thickness L on front-side (A) and back-side (B) illumination in the visible. J_0 (photons m^{-2} s^{-1}) is the intensity of light entering the bilayer.

Substitution in eq 5 for $\Delta\sigma(z)$ from eqs 6 and 7 results therefore in

$$\frac{\Delta P}{P} = -KeI_0 \sum \mu \int_0^L \phi_{CS}(z)\, \partial F_A(z) \tag{8}$$

For a single-component, homogeneous film, ϕ_{CS} will be independent of depth and eq 8 reduces simply to

$$\frac{\Delta P}{P} = -KeI_0 \phi_{CS} F_A \sum \mu \tag{9}$$

Defining the parameter $\eta = \phi_{CS}F_A$ as the quantum efficiency for charge separation per incident photon (the "IPCSE" value) and rearranging eq 9 results in the following relationship for $\eta\Sigma\mu$ in terms of the experimentally determined parameters $[\Delta P/P]$ and I_0.

$$\eta \sum \mu = -\frac{\Delta P/P}{KeI_0} \tag{10}$$

The results of FP-TRMC measurements are usually presented in terms of the $\eta\Sigma\mu$ parameter as given by eq 10.

Semiconductor/Antenna Bilayer. A change in conductivity of a TiO_2/antenna bilayer on irradiation in the visible region, where direct absorption by TiO_2 is negligible, can result from the diffusion of excited states formed within the antenna layer to the antenna/semiconductor interface followed by interfacial charge separation and injection of an electron into the semiconductor conduction band. The resulting value of $\eta\Sigma\mu$ is then given by

$$\eta \sum \mu = \eta_A \mu(e^-)_{SC} \tag{11}$$

with $\mu(e^-)_{SC}$ the mobility of conduction band electrons in the semiconductor and η_A the efficiency of interfacial charge separation per incident photon, given by

$$\eta_A = (1 - F_R)\phi_{inj} S \tag{12}$$

In eq 12, F_R is the fraction of incident photons reflected by the sample, S is the fraction of these photons that results in the

formation of excited states within the antenna layer which reach the TiO_2 interface by diffusion prior to their natural decay, and ϕ_{inj} is the probability that electron injection occurs on reaching the interface in competition with other deactivation processes.

The basic problem of exciton diffusion to an interface arose many years ago during attempts to determine the exciton diffusion coefficients, *D*, in aromatic crystals from surface fluorescence quenching measurements.[41] The problem was first solved mathematically by Simpson[40] for the condition illustrated in Figure 5A, which corresponds to "front-side" illumination in our terminology. Under these conditions the following differential rate equation applies.

$$\left[\frac{\partial n(z)}{\partial t}\right]_F = \alpha J_0 e^{-\alpha z} - \frac{n(z)}{\tau} + D\frac{\partial^2 n(z)}{\partial z^2} \qquad (13)$$

In eq 13, $n(z)$ is the exciton concentration at a depth z within the antenna layer, τ is the lifetime of excitons in the absence of surface quenching, and J_0 is the light intensity, in photons per unit area per second, penetrating the antenna layer. For back-side illumination, illustrated in Figure 5B, the corresponding rate equation is

$$\left[\frac{\partial n(z)}{\partial t}\right]_B = \alpha J_0 e^{-\alpha(L-z)} - \frac{n(z)}{\tau} + D\frac{\partial^2 n(z)}{\partial z^2} \qquad (14)$$

Under steady-state conditions, that is, $\delta n/\delta t = 0$, eqs 13 and 14 become nonhomogeneous, second-order, linear differential equations of the general form $y'' - \lambda y = Ce^{\gamma z}$, which can be solved by the method of "undetermined coefficients" to yield

$$n(z)_F = Ae^{-z/[(D\tau)^{1/2}]} + Be^{z/[(D\tau)^{1/2}]} - \frac{\alpha\tau J_0}{\alpha^2 D\tau - 1}e^{-\alpha z} \qquad (15)$$

and

$$n(z)_B = Ae^{-z/[(D\tau)^{1/2}]} + Be^{z/[(D\tau)^{1/2}]} - \frac{\alpha\tau J_0}{\alpha^2 D\tau - 1}e^{-\alpha(L-z)} \qquad (16)$$

The steady-state condition underlying the derivation of eqs 15 and 16 can be taken to apply in the present flash-photolysis experiments, since the exciton lifetime of 300 ps[49] is much shorter than the 3 ns pulse length.

To derive the relevant values of *A* and *B* in eqs 15 and 16, boundary conditions at the antenna layer surface and the antenna/semiconductor interface, that is, at $z = 0$ and $z = L$, respectively, must be defined. We make the assumption that excitons are rapidly deactivated on reaching the semiconductor interface, that is, at $n(L) = 0$. For the surface at $z = 0$ we consider two possibilities: either excitons are reflected, corresponding to $D(\delta n/\delta z) = 0$, or they are rapidly quenched, corresponding to $n(0) = 0$. While the former assumption would seem reasonable for pure crystalline layers of aromatic molecules, we cannot exclude the possibility that surface states of the polymer used in the present work could act as exciton quenching sites. Furthermore, in practical photovoltaic device structures the antenna layer would be coated with an electrode material, which would be expected to deactivate excited states. The two possibilities at $z = 0$ we denote below by subscripts R and Q, respectively, to indicate surface reflection or quenching.

The fraction *S* of photons entering the film that results in the formation of excitons which reach the semiconductor interface by diffusion is given by the magnitude of $-D[\delta n/\delta z]/J_0$ evaluated at $z = L$. This results in the following four relationships for *S*, of which eqs 17 and 19, for front- and back-side irradiation with a reflective surface, are identical to those derived earlier by Simpson[40] and Södergren,[50] respectively.

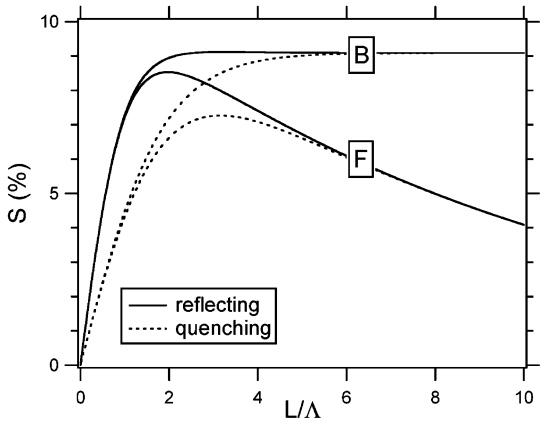

Figure 6. Calculated values of S according to eqs 17−20 plotted as a function of L/Λ for an exciton diffusion length one tenth of the photon penetration depth (i.e., $\Lambda = 0.1/\alpha$). The four curves correspond to front-side (F) and back-side (B) illumination with a reflecting (full lines) or quenching (dashed lines) antenna/gas interface.

$$S_{FR} = \left(\frac{\alpha^2\Lambda^2}{\alpha^2\Lambda^2 - 1}\right)\left(\operatorname{sech}\left(\frac{L}{\Lambda}\right) - e^{-\alpha L}\left(1 + \frac{\tanh\left(\frac{L}{\Lambda}\right)}{\alpha\Lambda}\right)\right) \qquad (17)$$

$$S_{FQ} = \left(\frac{\alpha^2\Lambda^2}{\alpha^2\Lambda^2 - 1}\right)\left(\frac{\operatorname{csch}\left(\frac{L}{\Lambda}\right) - e^{-\alpha L}\coth\left(\frac{L}{\Lambda}\right)}{\alpha\Lambda} - e^{-\alpha L}\right) \qquad (18)$$

$$S_{BR} = \left(\frac{\alpha^2\Lambda^2}{\alpha^2\Lambda^2 - 1}\right)\left(1 - e^{-\alpha L}\operatorname{sech}\left(\frac{L}{\Lambda}\right) - \frac{\tanh\left(\frac{L}{\Lambda}\right)}{\alpha\Lambda}\right) \qquad (19)$$

$$S_{BQ} = \left(\frac{\alpha^2\Lambda^2}{\alpha^2\Lambda^2 - 1}\right)\left(1 + \frac{e^{-\alpha L}\operatorname{csch}\left(\frac{L}{\Lambda}\right) - \coth\left(\frac{L}{\Lambda}\right)}{\alpha\Lambda}\right) \qquad (20)$$

In eqs 17−20 the combined parameter $\sqrt{(D\tau)}$ has been replaced by Λ, the "exciton diffusion length". The root-mean-square diffusion distance, Λ_d, is related to Λ by $\Lambda_d = \Lambda\sqrt{(2d)}$ with *d* the dimensionality.

Calculated values of *S* for all four combinations are plotted as a function of L/Λ in Figure 6 for the condition $\Lambda = 0.1/\alpha$, that is, an exciton diffusion length one tenth of the photon penetration depth, $\Lambda_{h\nu}$. Certain general points can be drawn from these plots: (a) the values of *S* for back-side irradiation both tend to the same limit of $\alpha\Lambda/(1 + \alpha\Lambda)$ for large L/Λ, (b) For front-side irradiation *S* decreases according to $\alpha\Lambda \exp[-\alpha L]/(1 - \alpha\Lambda)$ for large L/Λ and $\alpha\Lambda < 1$, and (c) S_{FR} passes through a maximum at a smaller value of L/Λ than that for the maximum of S_{FQ}. In the following section the above relationships for *S* are used in eq 12 to fit the thickness dependences of η_A observed in the present work, from which values of Λ and ϕ_{inj} are derived.

As mentioned above, the steady-state condition $\tau \ll \Delta t$, on which eqs 17 to 20 are based, is fulfilled for the present bilayers with the ~3 ns long pulses used. However, for antenna layers with natural exciton lifetimes of a nanosecond or longer, this will not be the case. This situation is dramatically illustrated by our recent results on metallo-porphyrin/TiO_2 bilayers where triplet sensitization can play an important role and can actually result in a growth of the photoconductivity for many micro-

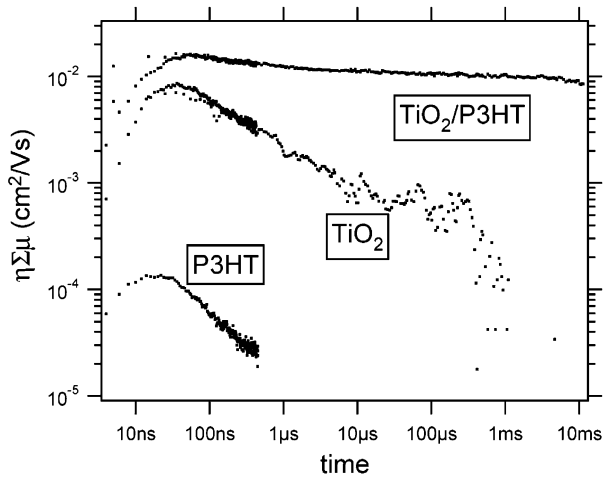

Figure 7. Transient changes in the conductivity on back-side flash-photolysis at 540 nm of a TiO_2/P3HT bilayer and layers of TiO_2 and P3HT alone. Note the logarithmic conductivity scale and time scale.

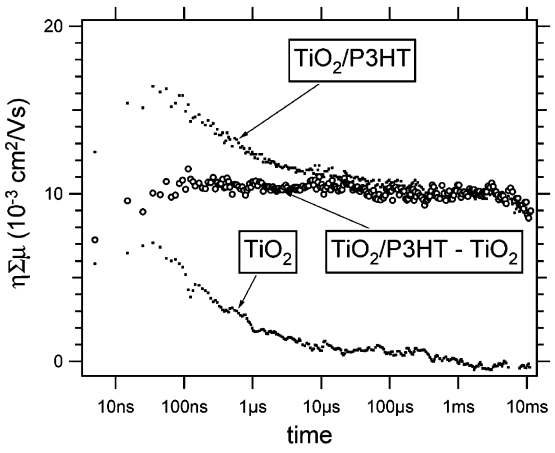

Figure 8. Photoconductivity transients shown in Figure 7 for back-side illumination of a TiO_2/P3HT bilayer and a bare TiO_2 layer at 540 nm plotted on a linear vertical scale for more ready comparison. Also included is the transient (circles) obtained by subtraction of the latter from the former.

seconds after the laser pulse.[51] Clearly, under these conditions steady-state assumptions are invalid. The above derivations are also inapplicable for relatively high light intensities where bimolecular, interexcitonic interactions have to be taken into account in the rate equations. These two "complications" can only be incorporated by applying numerical treatments of the exciton diffusion dynamics, which provide time-resolved solutions. We have developed such numerical treatments of the interfacial diffusion problem, and these will be published separately. Suffice to say that when steady-state conditions are simulated, the thickness dependences are practically identical to those given by the analytical approximations (eqs 17 to 20).

Results and Discussion

Optical Properties. The absorption spectra of a TiO_2/P3HT bilayer and separate TiO_2 and P3HT layers are shown in Figure 2. The bilayer spectrum can be reconstructed from the sum of the spectra of the separate layers and is independent of whether the sample is illuminated from the front (organic film) side or the back (TiO_2) side of the sample, apart from a slight difference in the 360−420 nm region. Of particular importance in the analysis of the photoconductivity data is that TiO_2 has only a very weak absorption in the wavelength region of the first absorption band of P3HT. On the other hand, the absorption by the polymer close to 300 nm, where the TiO_2 absorbs strongly (OD > 2), is relatively weak. This makes it possible to directly compare the conductivity resulting from photon absorption in the polymer layer in the visible with that resulting from direct band-gap excitation of the semiconductor in the UV under identical experimental and sample conditions.

The spectra of P3HT layers alone, shown in Figure 3, display a slight shift in the absorption maximum from 540 to 520 nm as the layer thickness increases from 16 to 230 nm. This effect has been observed previously by others for regioregular P3HT films and has been attributed to a certain degree of (pre)-aggregation in the higher concentration solutions used for spin-coating the thicker layers.[33,52] As pointed out below, this could possibly be the reason for the higher relative photoconductivity observed at shorter wavelengths in the bilayers.

Photoconductivity Transients. Conductivity transients observed on photoexcitation at 540 nm of a TiO_2/P3HT bilayer and separate layers of TiO_2 and P3HT alone are shown in Figure 7. The photoconductivity of the bilayer is seen to be considerably larger than that for either of the single layers alone, particularly at longer times. This provides direct evidence for sensitization of the semiconductor (i.e. formation of conduction band electrons) by light absorbed in the organic layer.

The photoconductivity observed for the bare TiO_2 layer at 540 nm is attributed to the direct formation of conduction band electrons by sub-band-gap excitation: process 6 in Figure 1B. This results in the formation of both electrons and their positively charged counterions within the TiO_2 layer itself, which is thought to be the reason for the relatively rapid decay via charge recombination in this case.

That a measurable photoconductivity is observed at all on irradiation of the bare TiO_2 layer in the visible, despite the very low attenuation of photons, is due to the high quantum yield of conduction band electrons formed by sub-band-gap excitation. Because of this, a contribution η_{SC} to the overall value of η from this source is observed on excitation of the bilayer samples in the visible. This can be seen in Figure 8, where the transients for back-side irradiation of a TiO_2/P3HT bilayer and the bare TiO_2 layer are compared. The early time decay for the bilayer sample is seen to follow the same decay kinetics as that for TiO_2 alone. Accordingly, we have subtracted the transient found for the TiO_2 single layer from that for the bilayer in order to obtain the "corrected" photoconductivity transient due to photon absorption in the organic layer alone. This transient is shown in Figure 8 and is seen to remain constant out to milliseconds after the pulse. Similar long-lived interfacial charge separation has been observed by others.[15,53]

Photoconductivity Action Spectra. The assignment of the long-lived photoconductivity to energy initially absorbed in the organic layer is corroborated by the good agreement between the wavelength onset of the photoconductivity and that of the absorption of P3HT, as shown in Figure 9. The results therefore conclusively support a mechanism whereby photoexcitations ("excitons") in the organic layer can diffuse to the semiconductor interface and inject electrons into the conduction band. The long lifetime of the conductivity can be explained if there is a substantial barrier to interfacial charge recombination: process 5 in Figure 1B.

The wavelength dependence of $\eta_A \Sigma\mu$ in Figure 9 is seen to follow the form of the attenuation spectrum from 650 nm down to approximately 550 nm, indicating a constant quantum yield for charge separation in this wavelength region. Below 550 nm there is however a slight positive deviation of $\eta\Sigma\mu$ from F_A, suggesting that an increase in the efficiency occurs at shorter

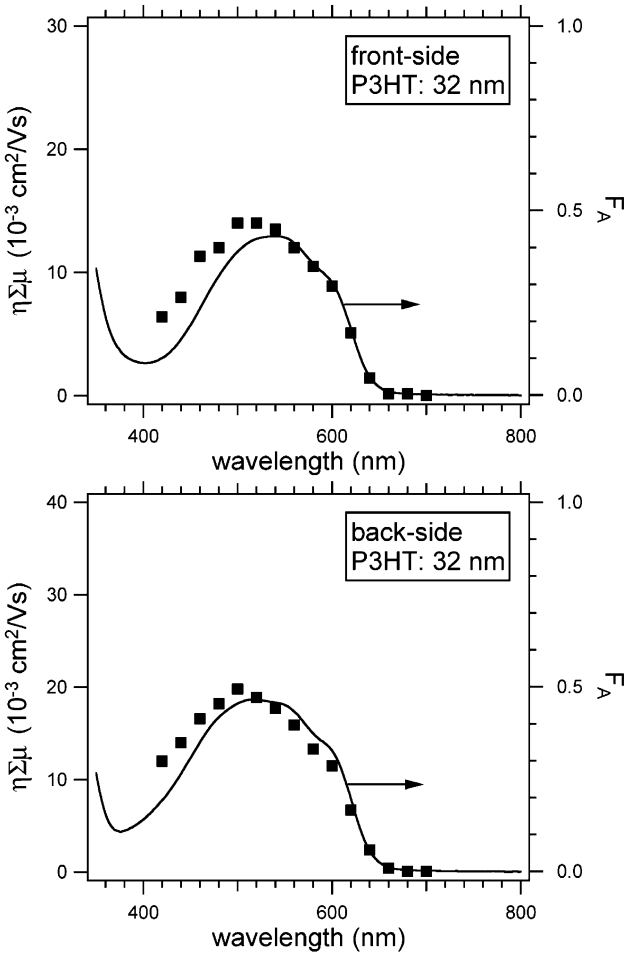

Figure 9. Wavelength dependence of the photoconductivity of a TiO_2/P3HT bilayer in the visible region (squares) and the fraction of incident photons absorbed in the sample (full line) for a polymer layer 32 nm thick on front-side (upper) and back-side (lower) irradiation. The conductivity has been corrected for a sub-band-gap contribution from the TiO_2.

wavelengths. This may be related to the hypsochromic shift in the absorption spectrum of P3HT layers with increasing thickness shown in Figure 3. This has been attributed to preaggregation in the solutions used for spin-coating.[33,52] It is possible therefore that light of shorter wavelengths is to a certain extent absorbed in better organized regions which support a longer exciton diffusion length and hence a higher overall charge separation efficiency.

Layer Thickness Dependence. In Figure 10 the thickness dependence of η_A, determined at close to the maximum of the P3HT absorption, is plotted as a function of layer thickness for both front- and back-side illumination. The full lines in Figure 10 are calculated fits to the experimental data using eq 12. The value of F_R in eq 12, determined spectrophotometrically, was independent of thickness and equal to 12% and 8% for front- and back-side illumination, respectively. The *S* parameters used were those for a reflective polymer/gas interface, that is, eqs 17 and 19. Equally good fits, within the error limits of the experimental data, could be obtained assuming a quenching polymer surface and using eqs 18 and 20. With α known (1.6×10^7 m^{-1}), the *form* of the antenna layer thickness dependence is determined exclusively by the exciton diffusion length, Λ. From the best fits, particularly to the data for front-side illumination which display a maximum, values of $\Lambda = 5.3$ or 2.6 nm were found, depending on whether a reflecting or quenching polymer surface was assumed. Having estimated Λ from the form of the thickness dependence, the value of the interfacial injection efficiency, ϕ_{inj}, was adjusted to give the best overall fit to the absolute magnitude of the IPCSE. The values of ϕ_{inj} corresponding to the above values of Λ were 12% and 25%, respectively.

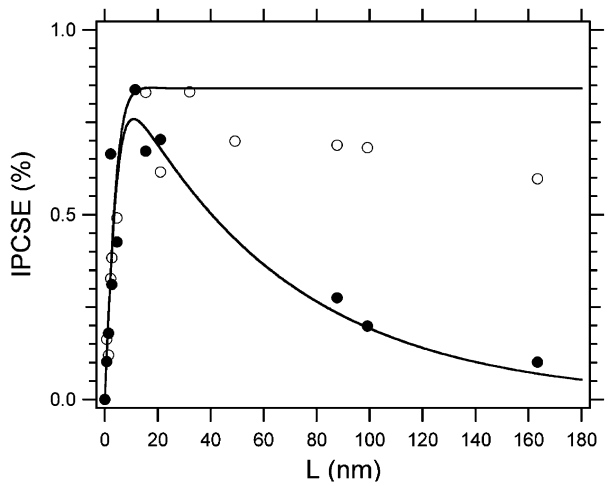

Figure 10. Dependence of the incident photon to charge separation efficiency (IPCSE) on the P3HT layer thickness for front-side (filled circles) and back-side (open circles) illumination. The full lines were calculated using eqs 17 and 19 with an optical absorption coefficient of 1.6×10^7 m^{-1}, an exciton diffusion length of 5.3 nm, and an efficiency for interfacial electron injection of 12%.

As can be seen, the experimental points for the thickest layers are lower than the calculated curve for back-side illumination. This could be due to a decrease in the absorption coefficient at 540 nm, by approximately 20%, as the layer thickness increases. Unfortunately, we were unable to carry out sufficiently accurate measurements of the layer thickness using the Dektak step-profiler for the thinner samples in order to be able to verify whether α did in fact decrease by this amount.

The values of Λ determined are in reasonable agreement with other estimates of the exciton diffusion length of close to 5 nm in polythiophene derivatives made by completely different experimental methods.[27,45] They are however considerably smaller than the value of ~20 nm found for poly(phenylene vinylene) derivatives.[11,43,44]

The redox properties of polythiophenes indicate that the LUMO of the polymer should lie approximately 0.4 eV above the conduction band of anatase.[54,55] The low value of ϕ_{inj} found could be due to other exciton deactivation pathways at the interface which compete effectively with charge injection into the semiconductor layer. A second possibility is that, despite the 0.4 eV exothermicity, there is a barrier to interfacial charge transfer,[56] which results in a lifetime toward electron injection which is considerably longer than the natural decay time of 300 ps. A study on nanoporous TiO_2 electrodes coated with similar polythiophenes has in fact shown that only partial quenching of the polythiophene luminescence occurs.[14]

Photoconductivity Action Spectra Revisited. As mentioned previously, the measured photoconductivity action spectra for the 32 nm layer follow closely the optical attenuation spectrum, $F_A(\lambda)$, for both front- and back-side illumination, as shown in Figure 9. This however is not the case for much thicker films upon front-side illumination, as is shown for an 88 nm thick film in Figure 11. Not only is the magnitude of η_A considerably lower for front-side compared with back-side illumination, as can be deduced from the thickness dependence relationships in eqs 17−20 for large *L*, but also the spectral form no longer

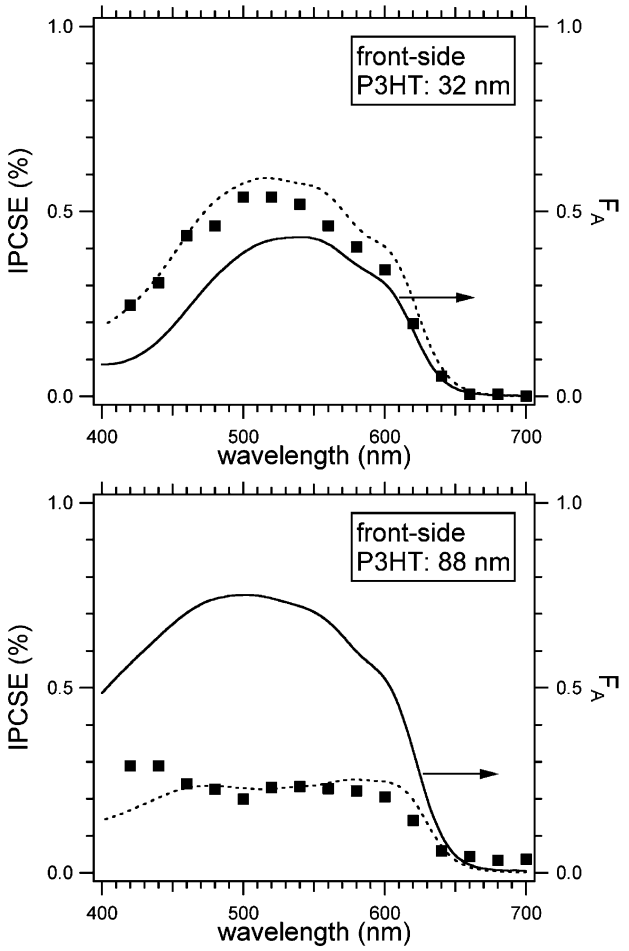

Figure 11. Wavelength dependence of the photoconductivity of a bilayer with P3HT layer thickness 32 nm (upper) and 88 nm (lower) for front-side illumination (squares). The full lines are the fraction of incident photons absorbed in the sample. The dashed lines are the calculated action spectra using eq 17 together with the measured wavelength dependence of α, given by $\alpha(\lambda) = \mathrm{OD}(\lambda)\ \ln 10/L$, and an exciton diffusion length of 5.3 nm and an efficiency for interfacial electron injection of 12%.

follows $F_A(\lambda)$ in the case of front-side illumination. This can be understood since, according to eqs 17−20, η_A depends on the value of the absorption coefficient, α, which is wavelength-dependent. For thicker layers, optical filtering effects occur on front-side illumination, resulting in decreased observed values for η_A.[57]

The spectral dependence actually expected for a given thickness L can be calculated by substituting for $\alpha = \mathrm{OD}(\lambda)\ \ln 10/L$ in eqs 17−20 using the measured optical absorption spectrum for this thickness. The predicted photoconductivity action spectra for the 32 and 88 nm samples, taking $\Lambda = 5.3$ nm and $\phi_{inj} = 0.12$, are shown as the dashed lines in Figure 11. Good agreement between the experimental and calculated action spectra for both the absolute magnitude and spectral form of η_A is observed.

Intensity Dependence. The effect of increasing the incident light intensity on charge separation has been studied from 0.54 to 66 μJ/cm^2 per pulse ($I_0 = 1.5 \times 10^{12}$ to 1.8×10^{14} photons/cm^2) for back-side irradiation at 540 nm of a 32 nm thick P3HT layer, and the results are shown in Figure 12. The IPCSE is seen to remain reasonably constant up to $\sim 2 \times 10^{13}$ photons/cm^2 but decreases gradually above this value. The action spectra in Figures 9 and 11, which were obtained for $I_0 \approx 1.5 \times 10^{13}$ photons/cm^2, correspond therefore to the intensity-independent

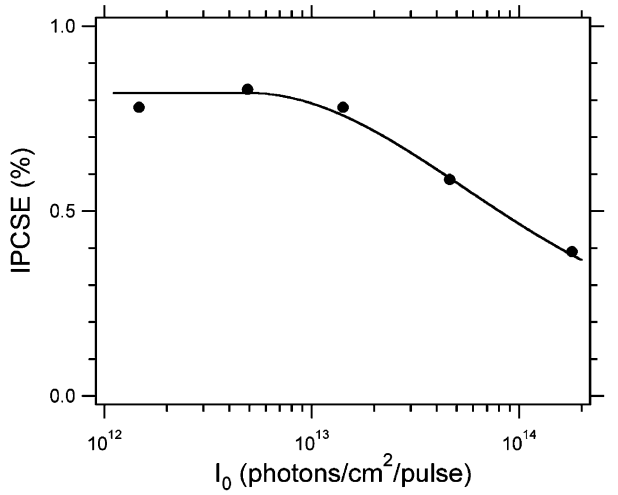

Figure 12. Intensity dependence of the charge separation efficiency per incident photon for back-side irradiation at 540 nm of a bilayer consisting of ~80 nm of TiO_2 and 32 nm of P3HT.

region. The decrease in IPCSE at higher intensities could be due to either the occurrence of exciton−exciton annihilation within the antenna layer, resulting effectively in a decrease in the exciton lifetime, or the increased buildup of charge at the semiconductor/polymer interface, resulting in an electric field gradient which retards interfacial electron transfer. We favor the former explanation on the basis of the following.

Effects due to exciton−exciton annihilation would be expected to become apparent for the condition that the rate of this process exceeds approximately 10% of the natural, unimolecular exciton decay rate, $1/\tau$, that is,

$$4\pi R D n_E > 0.1/\tau \qquad (21)$$

with R the reaction radius and n_E the exciton concentration. Since the average exciton concentration is given approximately by $n_E \approx \alpha I_0$, eq 21 corresponds to the following condition for the value of I_0 above which a decrease in efficiency due to exciton annihilation would be expected to occur.

$$I_0 > 0.1/4\pi R \Lambda^2 \alpha \qquad (22)$$

Taking for the reaction radius a value of 0.5 nm together with the measured value of $\alpha = 1.6 \times 10^7$ m^{-1} and an average value of $\Lambda = 4$ nm, effects due to exciton annihilation would be expected for I_0 larger than 0.6×10^{13} photons/cm^2 per pulse. This is in agreement with the decrease in charge separation efficiency shown in Figure 12 for I_0 values higher than approximately 1×10^{13} photons/cm^2 per pulse.

Conclusions

The flash-photolysis time-resolved microwave conductivity technique (FP-TRMC) has been used to study photoinduced charge separation in bilayers consisting of a smooth, transparent, 80 nm thick layer of anatase TiO_2 onto which poly(3-hexylthiophene), "P3HT", sensitizer layers have been spin-coated. The transient photoconductivity was monitored from nanoseconds to milliseconds following a single, 3 ns pulse using a digitizer with a logarithmic time base. Interfacial charge separation, after interfacial electron injection, was found to persist well into the millisecond time domain.

Photoconductivity action spectra have been measured between 420 and 700 nm for P3HT layer thicknesses, L, from a few to ~200 nanometers. Up to $L \approx 30$ nm the action spectrum

followed the photon attenuation spectrum with a maximum at a wavelength of ~540 nm. The efficiency of polymer-sensitized interfacial charge separation per incident photon (the "IPCSE") has been determined by comparing the photoconductivity on excitation in the visible with that on direct band-gap excitation of the anatase layer in the UV under identical experimental and sample conditions. Using this electrodeless technique, the IPCSE could be determined for illumination of a bilayer from either the polymer ("front") or semiconductor ("back") side.

On front-side irradiation at 540 nm (close to the absorption maximum of the polymer), the efficiency of charge separation per incident photon (IPCSE) initially increased to a maximum value of 0.8% for $L \approx 10$ nm. For thicker layers the IPCSE gradually decreased eventually to 0.1% for $L \approx 170$ nm. On back-side irradiation the IPCSE increased over the first 10 nm to a value close to the maximum found for front-side irradiation, and it decreased only slightly for further increase in layer thickness.

The thickness dependence of the IPCSE could be fitted using analytical expressions for exciton diffusion in combination with a Lambert−Beer excitation profile within the polymer layer. In addition to solutions for front- and back-side illumination, the possibilities that excitons are reflected or quenched at the polymer/gas interface were taken into account. From the fits to the experimental data, values of the exciton diffusion length, Λ, and the interfacial electron injection efficiency, ϕ_{inj}, could be determined. The values found were $\Lambda = 5.3$ or 2.6 nm and $\phi_{inj} = 12\%$ or 25% for a reflective or quenching gas interface, respectively. The low overall charge separation efficiencies found are therefore due to a combination of an injection efficiency considerably smaller than unity and an exciton diffusion length much smaller than the exponential photon penetration depth, which is 63 nm at the absorption maximum of the polymer.

The effect of incident light intensity was measured at 540 nm from 0.54 to 66 μJ/cm^2 (1×10^{12} to 2×10^{14} photons/cm^2) per pulse. The decrease in IPCSE found above approximately 10^{13} photons/cm^2 per pulse is attributed to the occurrence of exciton−exciton annihilation at higher light intensities.

An important aspect of the present measurements is that no electrodes are present. In addition to allowing the sample to be illuminated uniformly and equally from both sides, this avoids complications often found in real device structures resulting from exciton deactivation at the cathode, nonohmic electrode contacts, and pinhole defects. The intrinsic properties of the photoactive layer itself are therefore measured in the present work, and the value of the charge separation efficiency per incident photon (IPCSE) may be taken to be an upper limit for the incident photon conversion efficiency (IPCE) that would be expected in a photovoltaic cell for the same bilayer composition and excitation wavelength.

Acknowledgment. The authors wish to thank Prof. Dr. R. A. J. Janssen, Technical University of Eindhoven, for providing the P3HT and Dr. R. van de Krol, Delft University of Technology, for preparing the TiO_2 samples. The research was supported financially by The Netherlands Organization for Scientific Research (NWO).

References and Notes

(1) Sariciftci, N. S.; Smilowitz, L.; Heeger, A. J.; Wudl, F. *Science* **1992**, *258*, 1474.

(2) Karg, S.; Riess, W.; Meier, M.; Schwoerer, M. *Synth. Met.* **1993**, *57*, 4186.

(3) Sariciftci, N. S.; Braun, D.; Zhang, C.; Srdanov, V. I.; Heeger, A. J.; Stucky, G.; Wudl, F. *Appl. Phys. Lett.* **1993**, *62*, 585.

(4) Marks, R. N.; Halls, J. J. M.; Bradley, D. D. C.; Friend, R. H.; Holmes, A. B. *J. Phys.: Condens. Matter* **1994**, *6*, 1379.

(5) Yu, G.; Zhang, C.; Heeger, A. J. *Appl. Phys. Lett.* **1994**, *64*, 1540.

(6) Halls, J. J. M.; Pichler, K.; Friend, R. H.; Moratti, S. C.; Holmes, A. B. *Synth. Met.* **1996**, *77*, 277.

(7) Morita, S.; Lee, S. B.; Zakhidov, A. A.; Yoshino, K. *Mol. Cryst. Liq. Cryst. A* **1994**, *256*, 839.

(8) Yu, G.; Gao, J.; Hummelen, J. C.; Wudl, F.; Heeger, A. J. *Science* **1995**, *270*, 1789.

(9) Angadi, M. A.; Wasielewski, M. R. *J. Appl. Phys.* **1998**, *83*, 6187.

(10) Halls, J. J. M.; Walsh, C. A.; Greenham, N. C.; Marseglia, E. A.; Friend, R. H.; Moratti, S. C.; Holmes, A. B. *Nature* **1995**, *376*, 498.

(11) Savenije, T. J.; Warman, J. M.; Goossens, A. *Chem. Phys. Lett.* **1998**, *287*, 148.

(12) Salafsky, J. S.; Lubberhuizen, W. H.; Schropp, R. E. I. *Chem. Phys. Lett.* **1998**, *290*, 297.

(13) Arango, A. C.; Carter, S. A.; Brock, P. J. *Appl. Phys. Lett.* **1999**, *74*, 1698.

(14) van Hal, P. A.; Christiaans, M. P. T.; Wienk, M. M.; Kroon, J. M.; Janssen, R. A. J. *J. Phys. Chem. B* **1999**, *103*, 4352.

(15) Anderson, N. A.; Hao, E. C.; Ai, X.; Hastings, G.; Lian, T. Q. *Chem. Phys. Lett.* **2001**, *347*, 304.

(16) Breeze, A. J.; Schlesinger, Z.; Carter, S. A.; Brock, P. J. *Phys. Rev. B* **2001**, *6412*, art. no. 125205.

(17) Gebeyehu, D.; Brabec, C. J.; Sariciftci, N. S. *Thin Solid Films* **2002**, *403*, 271.

(18) Janssen, R. A. J.; Christiaans, M. P. T.; Hare, C.; Martin, N.; Sariciftci, N. S.; Heeger, A. J.; Wudl, F. *J. Chem. Phys.* **1995**, *103*, 8840.

(19) Janssen, R. A. J.; Christiaans, M. P. T.; Pakbaz, K.; Moses, D.; Hummelen, J. C.; Sariciftci, N. S. *J. Chem. Phys.* **1995**, *102*, 2628.

(20) Roman, L. S.; Andersson, M. R.; Yohannes, T.; Inganas, O. *Adv. Mater.* **1997**, *9*, 1110.

(21) Fromherz, T.; Padinger, F.; Gebeyehu, D.; Brabec, C.; Hummelen, J. C.; Sariciftci, N. S. *Sol. Energy Mater. Sol. Cells* **2000**, 61.

(22) Chen, L. C.; Roman, L. S.; Johansson, D. M.; Svensson, M.; Andersson, M. R.; Janssen, R. A. J.; Inganas, O. *Adv. Mater.* **2000**, *12*, 1110.

(23) Dittmer, J. J.; Marseglia, E. A.; Friend, R. H. *Adv. Mater.* **2000**, *12*, 1270.

(24) Sicot, L.; Fiorini, C.; Lorin, A.; Raimond, P.; Sentein, C.; Nunzi, J. M. *Sol. Energy Mater. Sol. Cells* **2000**, *63*, 49.

(25) Sharma, G. D.; Saxena, D.; Roy, M. S. *Synth. Met.* **1999**, *107*, 197.

(26) Granström, M.; Petritsch, K.; Arias, A. C.; Lux, A.; Andersson, M. R.; Friend, R. H. *Nature* **1998**, *395*, 257.

(27) Pettersson, L. A. A.; Roman, L. S.; Inganas, O. *J. Appl. Phys.* **1999**, *86*, 487.

(28) Kajihara, K.; Hirao, K.; Soga, N. *Jpn. J. Appl. Phys.* **1997**, *36*, 5537.

(29) Torsi, L.; Malitesta, C.; Sabbatini, L.; Zambonin, P. G.; Dodabalapur, A.; Katz, H. E. *Mater. Sci. Eng.* **1998**, *C5*, 233.

(30) Nogueira, A. F.; Micaroni, L.; Gazotti, W. A.; De Paoli, M. A. *Electrochem. Commun.* **1999**, *1*, 262.

(31) Rammelt, U.; Hebestreit, N.; Fikus, A.; Plieth, W. *Electrochim. Acta* **2001**, *46*, 2363.

(32) Luzzati, S.; Basso, M.; Catellani, M.; Brabec, C. J.; Gebeyehu, D.; Sariciftci, N. S. *Thin Solid Films* **2002**, *403*, 52.

(33) Yue, S.; Berry, G. C.; Green, M. M. *Macromolecules* **1996**, *29*, 6175.

(34) Granström, M.; Berggren, M.; Pede, D.; Inganas, O.; Andersson, M. R.; Hjertberg, T.; Wennerstrom, O. *Supramol. Sci.* **1997**, *4*, 27.

(35) Sirringhaus, H.; Brown, P. J.; Friend, R. H.; Nielsen, M. M.; Bechgaard, K.; Langeveld Voss, B. M. W.; Spiering, A. J. H.; Janssen, R. A. J.; Meijer, E. W.; Herwig, P.; de Leeuw, D. M. *Nature* **1999**, *401*, 685.

(36) Huang, H.; Pickup, P. G. *Chem. Mater.* **1999**, *11*, 1541.

(37) Neef, C. J.; Brotherston, I. D.; Ferraris, J. P. *Chem. Mater.* **1999**, *11*, 1957.

(38) O'Regan, B.; Grätzel, M. *Nature* **1991**, *334*, 737.

(39) Bach, U.; Lupo, D.; Comte, P.; Moser, J. E.; Weissortel, F.; Salbeck, J.; Spreitzer, H.; Grätzel, M. *Nature* **1998**, *395*, 583.

(40) Simpson, O. *Proc. R. Soc. London, Ser. A* **1957**, *238*, 402.

(41) Powell, R. C.; Soos, Z. G. *J. Lumin.* **1975**, *11*, 1.

(42) Gregg, B. A.; Sprague, J.; Peterson, M. W. *J. Phys. Chem.* **1997**, *101*, 5362.

(43) Becker, H.; Burns, S. E.; Friend, R. H. *Phys. Rev. B* **1997**, *56*, 1893.

(44) Savenije, T. J.; Vermeulen, M. J. W.; de Haas, M. P.; Warman, J. M. *Sol. Energy Mater. Sol. Cells* **2000**, *61*, 9.

(45) Theander, M.; Yartsev, A.; Zigmantas, D.; Sundstrom, V.; Mammo, W.; Andersson, M. R.; Inganas, O. *Phys. Rev. B* **2000**, *61*, 12957.

(46) van de Krol, R.; Goossens, A.; Schoonman, J. *J. Phys. Chem. B* **1999**, *103*, 7151.

(47) Wegewijs, B. R.; Dicker, G.; Piris, J.; Garcia, A. A.; de Haas, M. P.; Warman, J. M. *Chem. Phys. Lett.* **2000**, *332*, 79.
(48) de Haas, M. P.; Warman, J. M. *Chem. Phys.* **1982**, *73*, 35.
(49) Magnani, L.; Rumbles, G.; Samuel, I. D. W.; Murray, K.; Moratti, S. C.; Holmes, A. B.; Friend, R. H. *Synth. Met.* **1997**, *84*, 899.
(50) Södergren, S.; Hagfeldt, A.; Olsson, J.; Lindquist, S. E. *J. Phys. Chem.* **1994**, *98*, 5552.
(51) Kroeze, J. E.; Savenije, T. J.; Warman, J. M. *Adv. Mater.* **2002**, *14*, 1760.
(52) Kobashi, M.; Takeuchi, H. *Macromolecules* **1998**, *31*, 7273.
(53) Kroeze, J. E.; Savenije, T. J.; Warman, J. M. *J. Photochem. Photobiol.. A: Chem.* **2002**, *148*, 49.
(54) Guay, J.; Kasai, P.; Diaz, A.; Wu, R. L.; Tour, J. M.; Dao, L. H. *Chem. Mater.* **1992**, *4*, 1097.
(55) Abdou, M. S. A.; Orfino, F. P.; Son, Y.; Holdcroft, S. *J. Am. Chem. Soc.* **1997**, *119*, 4518.
(56) Zakhidov, A. A.; Yoshino, K. *Synth. Met.* **1994**, *64*, 155.
(57) Tang, C. W.; Albrecht, A. C. *J. Chem. Phys.* **1975**, *62*, 2139.